COMPUTER METHODS AND PROGRAMS IN BIOMEDICINE 108 (2012) 53–67

journal homepage: www.intl.elsevierhealth.com/journals/cmpb

Increasing sensitivity in the measurement of heart rate variability: The method of non-stationary RR time–frequency analysis

D. Melkonian[a,*], *A. Korner*[a], *R. Meares*[a], *H. Bahramali*[b]

[a] *Western Clinical School, University of Sydney, 5 Fleet Street, North Parramatta, NSW 2151, Australia*
[b] *Bioemotec, Sydney, NSW 2006, Australia*

ARTICLE INFO

Article history:
Received 18 August 2011
Received in revised form
3 January 2012
Accepted 9 January 2012

Keywords:
Heart rate variability
Non-stationary analysis
Spectral analysis
Fragmentary spectrum
SBF algorithm
RR deltagram
Controlled respiration

ABSTRACT

A novel method of the time–frequency analysis of non-stationary heart rate variability (HRV) is developed which introduces the fragmentary spectrum as a measure that brings together the frequency content, timing and duration of HRV segments. The fragmentary spectrum is calculated by the similar basis function algorithm. This numerical tool of the time to frequency and frequency to time Fourier transformations accepts both uniform and non-uniform sampling intervals, and is applicable to signal segments of arbitrary length. Once the fragmentary spectrum is calculated, the inverse transform recovers the original signal and reveals accuracy of spectral estimates. Numerical experiments show that discontinuities at the boundaries of the succession of inter-beat intervals can cause unacceptable distortions of the spectral estimates. We have developed a measure that we call the "RR deltagram" as a form of the HRV data that minimises spectral errors. The analysis of the experimental HRV data from real-life and controlled breathing conditions suggests transient oscillatory components as functionally meaningful elements of highly complex and irregular patterns of HRV.

1. Introduction

The variation in the timing between beats of the cardiac cycle, known as heart rate variability (HRV), has been shown to provide important insights into the balance between the two limbs of the autonomic nervous system, the sympathetic and parasympathetic branches [1]. This information has been widely used to assess the influence of the autonomic nervous system on cardiovascular control [2]. This has potential clinical significance for a variety of medical conditions, both of cardiac (myocardial infarction, congestive heart failure, life threatening arrhythmias, etc.) and non-cardiac origin (diabetes, neuropathies, obesity, etc.) [3]. Non-clinical applications include tests and monitoring of human performance under different physical and psychophysiological conditions [4]. A relatively novel field of HRV applications is the analysis of emotion regulation and psychological wellbeing, as outlined in the polyvagal theory [5].

Standard methods of HRV estimation are based on the measurement of intervals between heart beats using peaks of R waves in the electrocardiogram (ECG) as markers. One advantage of HRV based methodologies is that many of the commercial devices that are available perform automated measurement of inter-beat intervals. This means that they allow a relatively simple, non-invasive technique to be applied, thus broadening the potential range of applications for this form of measurement.

* *Corresponding author*. Tel.: +61 296182228.
E-mail address: dmitri@med.usyd.edu.au (D. Melkonian).
0169-2607/$ – see front matter © 2012 Elsevier Ireland Ltd. All rights reserved.
doi:10.1016/j.cmpb.2012.01.002

The extraction and evaluation of physiologically relevant information from HRV data is supported by both the time and frequency domain methods [6]. The conventional frequency domain measure is the power spectrum of HRV [3]. Consistently identified features of this spectrum are a low-frequency (LF) component centered around 0.1 Hz (frequency band between 0.04 and 0.15 Hz) and a high-frequency (HF) component which usually appears in the frequency band between 0.15 Hz and 0.5 Hz [3,7]. A large body of literature suggests that HF spectrum may be a reliable marker of the vagal control of heart rate in unstressed conditions and that LF may be a marker of sympathetic activity, or combined vagal and sympathetic activity, often encountered in relatively stressful circumstances [8]. For this type of application, frequency domain measures are thought to be more selective for evaluation of the relative contributions of sympathetic and parasympathetic function in cardiac regulation than time domain parameters.

The power spectrum assumes the stationarity of data and delivers frequency domain parameters averaged over relatively long recordings of HRV. Thus, the Task Force of the European Society of Cardiology and the North American Society of Pacing Electrophysiology recommend applying spectral analysis to segments of 5-min [3]. In this context, the frequency domain parameters are regarded as measures of steady-state physiological conditions [9].

However, the steady-state measures are not suited to capture the heterogeneous properties of heart-beats. Typical aspects of non-stationarity are the presence of "patchy" patterns that change over time. The evidence of multiple pseudo-periodic and aperiodic components in such spreads of activity [10] has intensified the interest in the identification of specific patterns of HRV that may indicate dynamic aspects of the control functions of the autonomic nervous system.

The most common approach to this problem consists in the estimation of a time-dependent spectrum of HRV [11,12]. However, the time–frequency analysis of HRV signals represents a major methodological challenge, because conventional techniques of digital spectral analysis, such as the fast Fourier transform (FFT) [13], are not suited to short-term spectral decompositions. Among novel computational tools that extend the application of classical Fourier integrals to time–frequency analysis is the similar basis function (SBF) algorithm [14]. This has the following advantages over conventional FFT:

1. The transcription of the signal under analysis into a digital form accepts both uniform and non-uniform sampling intervals.
2. The algorithm is applicable to signal segments of arbitrary length due to an explicit treatment of discontinuities at the boundaries of the integration intervals. This eliminates the need for windows of spectral analysis, along with their distorting impact.

In this paper we use these properties of the SBF algorithm to addresses the HRV time series as a non-stationary process. Our aim was to develop algorithms of HRV time–frequency analysis that provide a means to detect the major frequency components and measure their frequency, timing and magnitude. A simultaneous consideration of characteristic HRV patterns in both frequency and time domains is expected to provide additional insights into the mechanisms of autonomic control of heart function and may subsequently be used to discriminate between different physiological conditions in both research and clinical settings.

2. Background

2.1. *The power spectrum of HRV*

The conventional frequency domain characteristic of HRV is the power spectrum (or spectral density) [3,7]. This and similar frequency domain measures of HRV have found various applications in a number of research and clinical studies [6]. Specific methodological problems with the estimation and interpretation of the HRV power spectrum arise from the fact that HRV data are not a traditional object of spectral analysis. The tools of digital spectral analysis are usually applied to the time series of different types of deterministic or stochastic processes. By contrast, the HRV power spectrum is associated not with the signal itself (the ECG) but the point process that indicates the timing of the maximums of the R wave in ECG records, i.e. the occurrence times of the heart beats. Such a process can be described by a train of Dirac delta functions and transformed to the frequency domain in the form of the "spectrum of counts" [15]. However, the major methods of HRV spectral analysis deal not with the times of the heartbeats, but rather with the inter-beat intervals that are derived from the ECG and termed RR intervals.

Conceptually, the spectral analysis should be addressed to some time function that describes how the length of the RR interval evolves over time. Such a function cannot be supported by an exact analytical description, and its choice is one of the central methodological challenges for unambiguous frequency domain representation of HRV data. In general terms, the sequence of RR intervals may be regarded as the sequence of real numbers $(f_1, \ldots, f_n, \ldots, f_N)$, where f_n is the length of the RR interval associated with the heartbeat indexed by "n", and N is the number of intervals. The simplest approach to spectral analysis regards $(f_1, \ldots, f_n, \ldots, f_N)$ as a time series, i.e. the signal samples taken at regular sampling intervals. On this basis, the spectrum of intervals is defined by the discrete Fourier transform (DFT), and computed numerically using the FFT [15]. However, the assumption of regularly spaced heart beats when an actual timing is irregular, means that dual character of the relationships between the time and the frequency domains established by the forward and inverse Fourier transforms is lost in this approach [16–18].

Intrinsically irregular intervals between heartbeats are taken into account by the RR tachogram that represents the succession of values of varying intervals occurring at non-equidistant sampling times [17]. The problem with conventional spectral analysis in this context is that the FFT is applicable to 2^n samples of a time series with regular sampling intervals. Therefore, the RR tachogram must be resampled using interpolating methods in order to estimate the evenly spaced samples from the irregularly spaced samples. A number of investigations indicate that interpolation errors

produced by re-sampling may cause specific distortions of the spectral estimates [17,18]. These errors, together with the errors induced by windowing and zero padding, introduce significant uncertainty into the accuracy of the frequency domain measures of HRV.

Apart from the FFT, autoregressive (AR) models and the Lomb–Scargle periodogram method have been applied to HRV spectral analysis [19,20].

The main advantage supporting the AR approach to HRV spectral analysis is improved flexibility in relation to the length of analysis epoch and selection of sampling points. A major drawback is a strong dependency of the accuracy of spectral estimates on the order of the AR model. An adequate selection of this parameter is ambiguous because the validity of the underlying assumptions has not as yet been proved [21].

The benefit of the Lomb–Scargle periodogram is that this method directly calculates the power spectrum from an unevenly sampled RR tachogram [20]. However, reliable performance of the method depends on a number of conditions that include specific relationships between the signal and noise. A comparison of different methods of HRV spectral analysis suggests that interpolation methods are better solutions than the direct Lomb method [18].

2.2. *SBF algorithm*

Numerical algorithms developed in this study are supported by a series of preceding investigations that addressed the problem of time–frequency analysis of non-stationary biomedical signals [22–24]. Given the Fourier integrals as basic computational tools, the major problem is that these transforms belong to a category of oscillatory integrals, and demand special algorithms for numerical integration. The estimation of trigonometric integrals with maximum degree of precision is provided by Filon-type methods, based on the polynomial expansion of the signal to be transformed [25]. However, the corresponding computational methods are not supported by effective algorithms and require tedious calculations. The objective guiding the development of the SBF algorithm was to support the Filon-type method of integration by an effective computational solution [14]. The algorithm decomposes the signal into the sum of self-similar finite elements with the simple analytical form of the frequency spectrum. Simultaneous consideration of both the time and frequency domains reduces the entire issue of the Fourier transform calculations to standard frequency domain manipulations with relatively simple analytical functions.

3. Design considerations

The algorithmic design in this paper is focused on the development of computational tools that support HRV time–frequency analysis through a simultaneous consideration of both the time and frequency domains. There are two related goals. The first is to transform selected segment of HRV data to the frequency domain. This provides means for the time–frequency analysis, i.e. the analysis of the time dependent frequency content of non-stationary HRV. However, short term spectral analysis is highly sensitive to spectral leakage which can distort spectral estimates. In this context, the result of the time–frequency analysis is useless unless the accuracy of spectral estimates can be judged. Thus, the second goal is to verify the success of the first goal. For this purpose we use inverse cosine or sine Fourier transform to restore the time domain counterpart of the frequency domain solution, and compare it with the initial time domain data.

We use the recipes of the SBF algorithm to support both goals by a universal computational technique. The data to which we apply the time to frequency transformation are derived from sequential instants $(t_0, \ldots, t_m, \ldots, t_M)$ at which the R waves are peaking. Such point events occurring haphazardly along a one dimensional time continuum may be described as a univariate point process. To apply Fourier transforms, we need to assign numbers to the event's occurrence times, i.e. to characterize each heart beat by a data point (t_m, f_m), where f_m is called a point event. Physically, we regard f_m as the value of some parameter $f(t)$ used to characterize the heart beats. A formal assumption is that $f_m = f(t_m)$. Taken a series of data points on the interval of interest, the general form of the data for analysis is the finite sequence of the data points $\mathbf{F}_t = \{(t_0, f_0), \ldots, (t_m, f_m), \ldots, (t_M, f_M)\}$. Irrespective of the choice of the point events, we may regard $\mathbf{F}_t$ as a discrete form of a certain continuous time function $f(t)$ called the point event function (PEF), and defined on the interval of finite length $L = t_M - t_0$.

Let t_j and $t_k > t_j$ be the boundary time points that define a particular segment of the PEF. The complex spectrum of the corresponding fragment of the PEF is defined by the following continuous finite Fourier integral

$$F(\omega) = \int_{t_j}^{t_k} f(t)\ \exp(-i\omega t)\, dt, \tag{1}$$

where $i = \sqrt{-1}$, $\omega = 2\pi f$, and f is the frequency.

Alternatively, we may describe the same fragment by the function $g(\tau) = f(t - t_j)$, associated with the data points $\mathbf{G}_\tau = \{(\tau_0, g_0), \ldots, (\tau_i, g_i), \ldots, (\tau_N, g_N)\}$, where $\tau_i = t_{i+j}$, $g_i = f_{i+j}$ and $N = k - j + 1$.. The complex spectrum is given by

$$G(\omega) = \int_0^{\lambda} g(\tau)\ \exp(-i\omega\tau)\, d\tau, \tag{2}$$

where $\lambda = t_k - t_j$.

In terms of real functions:

$$G(\omega) = G_C(\omega) - iG_S(\omega),$$

where

$$G_C(\omega) = \int_0^{\lambda} g(t)\ \cos\omega t\, dt, \qquad G_s(\omega) = \int_0^{\lambda} g(t) \sin\omega t\, dt. \tag{3}$$

The amplitude spectrum of $g(t)$, i.e. the module of the complex spectrum, is

$$\left|G(\omega)\right| = \sqrt{G_C^2(\omega) + G_S^2(\omega)}. \tag{4}$$

The time shift between $f(t)$ and $g(t)$ has no effect on the amplitude spectrum, i.e. $\left|F(\omega)\right| = \left|G(\omega)\right|$. This shows that although the spectral analysis is applied to segments of

different length and timing, the computational framework is essentially the same.

Both $G_C(\omega)$ and $G_S(\omega)$ contain information that allows restoration of $y(t)$ using the following inverse Fourier cosine and sine transforms:

$$g(t) = \frac{2}{\pi}\int_0^{\infty} G_C(\omega)\ \cos\omega t\, dt, \tag{5}$$

$$g(t) = \frac{2}{\pi}\int_0^{\infty} G_S(\omega)\ \sin\omega t\, dt. \tag{6}$$

Theoretically, the Fourier integrals of finite extent function $g(t)$ must be infinite in the frequency domain. This explains semi-infinite integration intervals in Eqs. (5) and (6). However, because we may associate $g(t)$ with a physically realizable stable system, the asymptotic behavior of the frequency characteristics in the high frequency ranges is such that both $G_C(\omega)$ and $G_S(\omega)$ decrease with increasing frequency. Therefore, it is always possible to find an angular frequency Ω above which $G_C(\omega)$ and $G_S(\omega)$ are negligibly small. On these grounds, the approximants to $g(t)$ may be estimated from the following finite cosine and sine Fourier transforms:

$$g(t) \approx g_C(t) = \frac{2}{\pi}\int_0^{\Omega} G_C(\omega)\ \cos\omega t\, dt, \tag{7}$$

$$g(t) \approx g_S(t) = \frac{2}{\pi}\int_0^{\Omega} G_S(\omega)\ \sin\omega t\, dt. \tag{8}$$

Let (3) and (4) be the spectral characteristics computed from the set of data points. We use (7) and/or (8) in order to ascertain the accuracy and reliability of the spectral estimates.

Comparison of these integrals with (3) shows that essentially the same methods may be used to perform the transformations from the time to frequency domain and vice versa. Computationally, we must be able to estimate trigonometric integrals the general form of which is:

$$Y_C(u) = \int_0^{\lambda} y(x)\ \cos ux\, dx, \tag{9}$$

$$Y_S(u) = \int_0^{\lambda} y(x)\ \sin ux\, dx. \tag{10}$$

These integrals are the point of departure for design of the HRV time–frequency analysis algorithms.

4. Method

4.1. *Numerical Fourier transforms*

We address numerical estimation of (9) and (10) to the set of data points $\mathbf{Y}_x = \{(x_0, y_0), \ldots, (x_i, y_i), \ldots, (x_N, y_N)\}$ with $x_0 = 0$ and $x_N = \lambda$. Using the basis functions of previously developed SBF algorithm [14], we establish the fundamental relationship between the data points and continuous $y(x)$ using the sum of finite elements

$$y(x) = \sum_{i=0}^{N-1} a_i\theta_i(x), \tag{11}$$

where a_i are the weighting coefficients, and $\theta_i(x)$ is a similar basis function (SBF). The SBF is defined by the similarity relationship

$$\theta_i(x) = r\left(\frac{x}{x_{i+1}}\right). \tag{12}$$

This simple parameterised time scaling produces the family of SBFs from a basic finite element

$$r(x) = \begin{cases} 1 - x & \text{if } \ 0 \le x \le 1 \\ 0 & \text{otherwise} \end{cases}$$

termed "triangular basis function" (TBF). The TBF is a unit right-angled triangle depicted in Fig. 1A.

With regard to the data points, $y(x)$ is a piecewise linear approximating function, defined by the following condition:

$$y(x_i) = y_i \text{ for } i = 0, 1, \ldots, N-1.$$

A similar transition from the data points to a continuous time function is used by resampling procedures of a number of the HRV spectral analysis methods [15,17,18]. In this context the $y(x)$ serves as an interpolation function the goal of which is to fill the intervals between the original data points by equidistant samples. This remedy of matching the HRV data to the demands of conventional FFT also includes the addition of zeros (zero padding) to achieve 2^n data points [15].

The advantage of the SBF algorithm is that the procedures of the spectral analysis are directly applied to the original data points, and are free of resampling.

In terms of finite elements, the approximant (11) may be presented in the form

$$y(x) = y_0\theta_0(x) + \sum_{i=1}^{N-1} y_i\phi_i(x), \tag{13}$$

where $\varphi_i(x)$ is a hat function.

Being a tool of the finite-element method [26], the hat function is defined as

$$\phi_i(x) = \begin{cases} \dfrac{x - x_{i-1}}{x_i - x_{i-1}}, & \text{if } x_{i-1} \le x < x_i \\ \dfrac{x_{i+1} - x}{x_{i+1} - x_i}, & \text{if } x_i \le x < x_{i+1} \\ 0, & \text{otherwise} \end{cases}$$

on the mesh $x_0 < x_1 < \ldots < x_i < \ldots < x_N$.

Fig. 2 exemplifies decomposition (13). The dotted lines connecting data points from 0 to 4 represent on the segment 'ad' the sum of the TBF (triangle a0b) and the hat functions (triangles a1c, b2d and c3e) with vertexes at the data points from 1 to 3.

The comparison of (11) and (13) shows that hat functions in (13) are replaced in (11) by TBFs. The geometrical principle

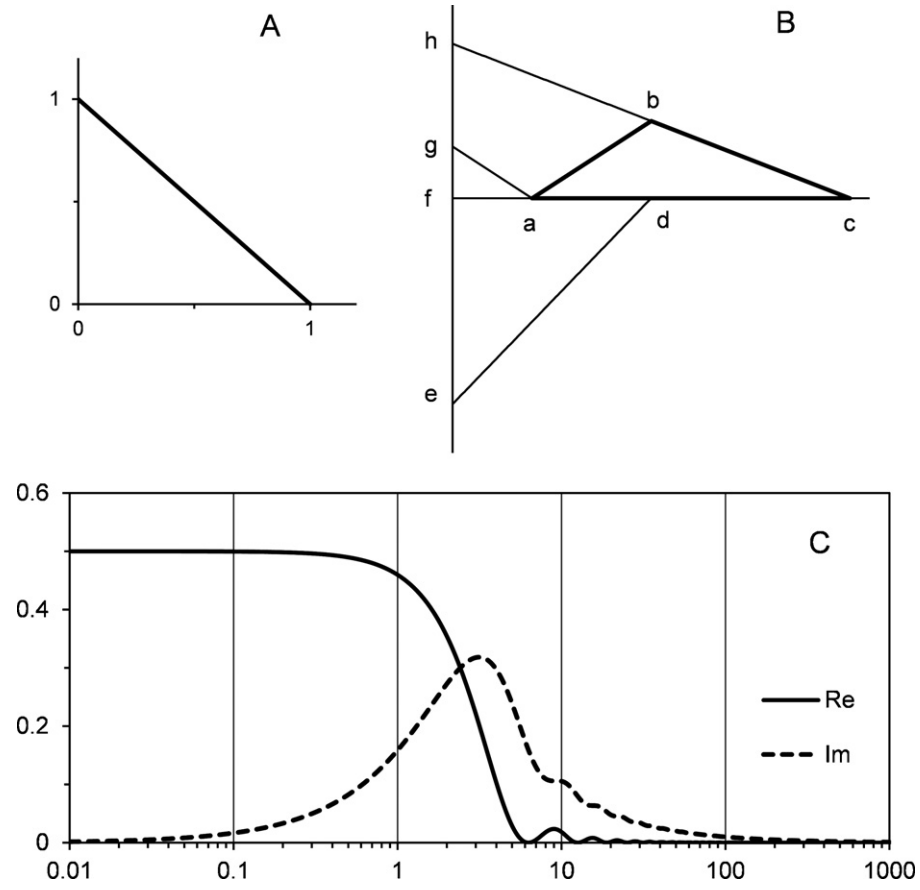

Fig. 1 – (A) Unit right-angled triangle. This finite element is the TBF from which an ensemble of similar basis functions is deduced. (B) Shows decomposition of the hat function (triangle abc) into the sum of SBFs (triangles fhc, fed and fga). (C) The curves Re and Im show the real and imaginary parts of the complex spectrum of the TBF, i.e. the functions (15) and (16), respectively.

found useful in this connection is illustrated by Fig. 1B. The graph shows the decomposition of the hat function (triangle abc) into the sum of three TBFs (triangles fhc, fed and fga). Application of this decomposition to all hat functions in (13) results in the following formula for the estimation of interpolation coefficients

$$\begin{aligned} a_i &= \alpha_i y_i - \beta_{i+1} y_{i+1} + \gamma_{i+2} y_{i+2},\ 0 \le i < N-3 \\ a_{N-2} &= \alpha_{N-2} y_{N-2} - \beta_{N-1} y_{N-1}, \\ a_{N-1} &= \alpha_{N-1} y_{N-1}, \end{aligned} \tag{14}$$

where

$$\begin{aligned} \alpha_i &= \frac{x_{i+1}}{\Delta x_{i+1}} && (0 \le i \le N-1), \\ \beta_i &= x_i \frac{\Delta x_{i+1} + \Delta x_i}{\Delta x_{i+1} \Delta x_i} && (1 \le i \le N-1), \\ \gamma_i &= \frac{x_{i-1}}{\Delta x_i} && (2 \le i \le N-1), \\ \Delta x_i &= x_i - x_{i-1}. \end{aligned}$$

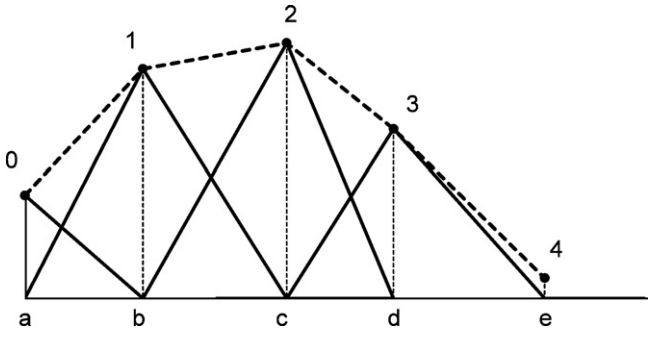

Fig. 2 – Exemplifies the transition from the data points (filled circles 0–4) to finite elements: SBF (vertex at the data point 0) and the hat functions with vertexes at the data points from 1 to 3. The dotted line shows the sum of finite elements.

In the context of numerical solutions, the chief advantage of the construction (11) is that cosine and sine Fourier integrals from the TBF are expressed in an analytical form as

$$R_C(u) = \int_0^\infty r(x)\ \cos(ux)\, dx = \frac{1-\cos u}{u^2}, \tag{15}$$

$$R_S(u) = \int_0^\infty r(x)\ \sin(ux)\, dx = \frac{u-\sin u}{u^2}. \tag{16}$$

Fig. 1C shows these functions.

According to the theory of Fourier transforms (similarity theorem), the compression of the abscissa in the time domain corresponds to the expansion of the abscissa plus the contraction of the ordinate in the frequency domain. Application of these operations to the functions (15) and (16) allows us to express Fourier transforms from (12) in the following form:

$$\int_0^\infty \theta_i(x)\cos ux\,dx = x_{i+1}R_C(x_{i+1}u),$$

$$\int_0^\infty \theta_i(x)\sin ux\,dx = x_{i+1}R_S(x_{i+1}u).$$

It follows rather straightforwardly from (11) that these formulas reduce calculations of (9) and (10) to the following standard operations with analytical functions (15) and (16)

$$Y_C(u) = \sum_{i=0}^{N-1} a_i x_{i+1} \frac{1-\cos(x_{i+1}u)}{(x_{i+1}u)^2}, \tag{17}$$

$$Y_S(u) = \sum_{i=0}^{N-1} a_i x_{i+1} \frac{ux_{i+1}-\sin(x_{i+1}u)}{(x_{i+1}u)^2}. \tag{18}$$

After estimation of the weighting coefficients from (14), these formulas are directly applied to the time points of the PEF in question.

4.2. *Fragmentary spectrum*

The technique of numerical Fourier transform described above provides means to express the complex spectrum (2) in terms of its real and imaginary parts (3). Each of these frequency characteristics contains the full amplitude and phase information necessary to restore the initial time domain function. However, a complicated form of these functions is inconvenient for display and direct measurements of the amplitudes of spectral components.

An appealing feature of the power spectrum is its ability to provide direct measures of different spectral components of the signal. For that reason the power spectrum is one of the most frequently applied frequency domain descriptors of HRV [3]. A major problem that opposes the analysis and interpretation of the power spectrum estimates is that HRV exhibits irregular patterns of activity, i.e. belongs to the category of non-stationary processes [3,6]. The main point at issue is that the power spectrum is defined in the field of probability and statistics as the frequency domain measure of a stationary random process [27]. Non-stationary processes are not supported by a strict definition of the power spectrum. To accentuate ambiguity raised by this inconsistency, suppose that $F_1(\omega)$, $F_2(\omega)$, ... are the power spectra computed over different segments of stochastic process $f(t)$. If $f(t)$ is stationary, spectral functions $F_1(\omega)$, $F_2(\omega)$, ..., may be regarded as the samples of a single random function $\mathbf{F}(\omega)$. In other words, $F_1(\omega)$, $F_2(\omega)$, ..., appear as ensemble functions allied by some probabilistic relationships. This concept is not applicable to non-stationary HRV.

To approach the problem of non-stationarity, we associate HRV with irregular stochastic process certain fragments of which may possess special properties of functional significance. To define this special class of PEF fragments in the frequency domain, we introduce a novel notion of the fragmentary spectrum that is a combination of the frequency and time domain descriptors of the PEF. Using the same notations as Eqs. (1)–(4), we regard $|t_k,t_j|$ segment of the PEF $\mathbf{G}_\tau$. The fragmentary spectrum is defined as

$$\mathbf{G}(f,\xi,\lambda) = \lambda^{-1}\left|\mathbf{G}(2\pi f)\right|, \tag{19}$$

where $\xi = t_j$ and $\lambda = t_k - t_j$. These parameters define the position and length of the corresponding segment of the PEF.

Compared with the power spectrum, a major advantage of the fragmentary spectrum is its ability to measure how spectral estimates evolve over time. However, if the underlying system is stationary, the fragmentary spectrum may be independent of ξ and λ. In this case the power spectrum is simply $P(f) = \mathbf{G}^2(f,\xi,\lambda)$.

The question we now consider is how to link the fragmentary spectrum with different patterns of HRV. With regard to the conventional power spectrum, measurements of spectral characteristics regard "peak" as a marker of a functional component. Physical and physiological interpretation of these components has been supported by the assumption of stationarity, i.e. the presence of continuous permanent rhythms of HRV [3,7,9].

By contrast, using notions of non-stationary processes, we can think of HRV as a reflection of discrete sources generating transient changes of inter-beat intervals. When we find a peak in the fragmentary spectrum $\mathbf{G}(f,\xi,\lambda)$ at certain frequency $f = f_M$ we know that the underlying signal contains an oscillatory component with frequency f_M in the time interval from ξ to $\xi+\lambda$. Given importance of oscillatory processes for spectral analysis, we shall call the corresponding component transient oscillatory component (TOC).

The resonant frequency serves as a primary marker of TOC. However, the location and length of the TOC, i.e. ξ and λ, are not known in advance, and we need additional information for an exact identification of TOC. For this purpose we estimate fragmentary spectra over a succession of different segments collected from the time window running through the PEF. Given the data points $\mathbf{G}_t = \{(t_0, y_0), \ldots, (t_m, y_m), \ldots, (t_M, y_M)\}$, we define the length of the moving window by the number of points $p < M/2$. The initial position of the window is defined by a sliding pointer, which is placed at $i = p$. From this position the pointer is moved within the data points until i takes the value $M-p$. For each position of the pointer fragmentary spectrum is estimated for preselected range of frequencies from F_{MIN} to F_{MAX}. The maximum resonant frequency f_M is regarded as the dominant frequency of TOC while ξ and λ parameters are defined by the window position and length.

Suppose we want to perform the moving window analysis over the time scale but are uncertain what the window size should be. We can start the procedure using a window of relatively short duration and then stretch the window out a small amount and compute another set of parameters, and so on, gradually increasing the window size and computing another set of frequency domain measures for each value of window

size. Inspecting many of these trials results in a comprehensive representation of the TOC in terms of its descriptive parameters.

4.3. RR deltagram

In Section 3 we have defined a general form of the data for spectral analysis as a finite sequence of the data points in the form of the PEF $\mathbf{F}_t = \{(t_0, f_0), \ldots, (t_m, f_m), \ldots, (t_M, f_M)\}$, where t_m ($m = 0,\ldots,M$) is the occurrence time of the heart beats. Given the inter-beat interval (RR interval) as a physical parameter of interest, the point event is expressed as $f_m = t_{m+1} - t_m$. Under this condition, the $\mathbf{F}_t$ represents the conventional RR tachogram [17] also known as a discrete event series [3].

An alternative approach to the spectral analysis design is supported by the view that the deviations of the RR intervals from the mean value rather than the length of the interval itself are basic to the characterization of HRV. The conclusion has been drawn that subtraction of the mean value of RR interval from the time series before applying the FFT increases the sensitivity of spectral estimates to the dynamics of HRV [18]. Previous studies applied this technique after replacement of irregularly spaced time points by regularly spaced time points. Here we approach digital spectral analysis in a way that avoids resampling. We introduce the RR deltagram as a PEF defined by the point event

$$f_m = \Delta t_m - e(t_m), \tag{20}$$

where $\Delta t_m = t_m - t_{m-1} (m = 1, \ldots, M)$ and $e(t)$ is the function that defines the expected value of RR interval.

We use the technique of moving window averaging to build the procedure for estimation of expected values of RR intervals. Compared with conventional applications of moving window averaging [28], a specific aspect of the problem is the non-even distribution of sampling intervals. This factor may induce a false high-frequency components in the spectrum of $e(t)$. To overcome this problem, we have designed a digital filtering algorithm which performs a multistep moving window averaging.

The algorithm deals with the sets of real numbers $\mathbf{E}^1 = \{e_0^1, \ldots, e_m^1, \ldots, e_M^1\}, \ldots$, $\mathbf{E}^k = \{e_0^k, \ldots, e_m^k, \ldots, e_M^k\}, \ldots$, $\mathbf{E}^K = \{e_0^K, \ldots, e_m^K, \ldots, e_M^K\}$, where the subscript ($m$ from 0 to M) denotes the number of the beat, and the superscript (k from 1 to K) indicates the number of step in the procedure of averaging.

The set $\mathbf{E}^k$ is the output of the kth step which further serves as an input of the $(k+1)$th step. To initiate this recursion we define the first set as the succession of Δt_m intervals from (20), i.e. $e_m^1 = \Delta t_m$. The transition from the set $\mathbf{E}^k$ to the set $\mathbf{E}^{k+1}$ ($k = 1,\ldots,K-1$) during recursion is defined by conventional procedure of the moving averaging with equal weights:

$$e_m^{k+1} = \frac{1}{n_L + n_R + 1} \sum_{j=-n_L}^{n_R} e_{m+j}^k, \tag{21}$$

where n_L and n_R are the numbers of the points to the left and right of the center of the window. The number of the data points captured by the window is $N_W = n_L + n_R + 1$.

The practical criterion that is the basis by which we accept a multistep average as a stable solution is the condition $\Delta E_{k+1} < T_E$, where

$$\Delta E_{k+1} = \frac{1}{n_L + n_R + 1} \sum_{m=0}^{M} \frac{\left| e_m^{k+1} - e_m^k \right|}{e_m^k},$$

is the mean of the absolute value of the normalised residual between the values of "e" at k and $k+1$ steps of recursion, and T_E is a threshold value for residual (default option is 0.01).

4.4. Inverse RR deltagram

The necessity of direct evaluation of the accuracy of the time to frequency transformations is critical to the time–frequency analysis because shortening of the epoch of analysis may drastically increase the role of factors, such as spectral leakage, that distort the form of the spectrum.

Using inverse Fourier transforms, our approach to the problem is straightforward. The question we pose is how accurate is the numerically computed fragmentary spectrum as a frequency domain counterpart of the corresponding deltagram? Let $G_C(\omega)$ and $G_S(\omega)$ in (7) and (8) represent the real and imaginary parts of the fragmentary spectrum in question. We may expect that numerical estimation of both (7) and (8) should reasonably restore the RR deltagram, although some error is involved.

This provides a universal method for evaluation of errors using the forward Fourier transform, followed by the inverse Fourier transform. The first step is the transition from the time to frequency domain using the forward FT. The second step is the restoration of the transient response from numerical frequency characteristics using the inverse FT. With regard to (7) and (8), we evaluate the accuracy of inverse transforms by residual functions $r_C(t) = g(t) - g_C(t)$ and $r_S(t) = g(t) - g_S(t)$. The residuals accumulate the errors of the forward time to frequency transformation (2) and inverse the frequency to time transformation (5) or (6). We can write this as

$$r_C(t) = r_{FC}(t) + r_{IC}(t) \quad \text{and} \quad r_S(t) = r_{FS}(t) + r_{IS}(t), \tag{22}$$

where $r_{FC}(t)$ and $r_{IC}(t)$ are associated with the forward and inverse cosine Fourier transforms, and $r_{FS}(t)$ and $r_{IS}(t)$ are associated with the forward and inverse sine Fourier transforms.

On these grounds, we use numerical estimation of the inverse Fourier transforms as a tool to test consistency between the time domain PEF and its frequency domain counterparts.

5. Results

The aim of this section was to ensure that developed algorithms worked properly and provided time dependent spectral measures of non-stationary HRV capable to detect and identify specific patterns of HRV. For this purpose we set up a technique for non-invasive recordings of HRV data on healthy subjects using a "Zephyr Bioharness" device for simultaneous wireless monitoring of ECG, heart rate and breathing waveforms. The measuring part of this device is strapped on like a belt and is a non-invasive instrument suitable for use in a naturalistic

setting. From the data produced by the microprocessor of the device, we selected for further off-line processing the values of RR intervals, digitized ECG and breathing waveforms.

The computer implementation of the developed algorithms for HRV data processing has been supported by specially designed software "RR_SBF" using the object Pascal language of Embarcadero Delphi 2010. The program contains a number of routines that support major algorithms described in the paper. Launching the data transfers and various computational tasks is governed by graphical user interface with windows, menus, charts and dialogs.

In order to detect and investigate specific patterns of HRV, the data were monitored on 8 healthy subjects under different conditions that include the rest, spoken conversation and controlled breathing.

5.1. *Computer experiments with RR deltagrams*

The aim of this section is a simultaneous consideration of HRV measures in both the time and frequency domains and the analysis of errors in these two domains. Based on the analysis of different sequences of RR intervals monitored under different experimental conditions, our objective is to show the advantages of the introduced RR deltagram over conventional RR tachogram. The point is that boundary discontinuities of conventional RR tachogram may have distorting impact on the transforms. The following analysis of this issue in computer experiments is general, and does not depend on the experimental conditions supporting the HRV monitoring. Our focus on the conditions of controlled breathing is explained by the fact that coupling of the heart beats with respiratory rhythms provides means to emphasize particular frequencies of the HRV spectra.

During the experiments with controlled breathing the subject used a metronome to count breaths while simultaneous recordings of breathing and RR intervals were done. Recordings were done at rest, during spoken conversation and during controlled respiration at breathing rates of approximately 5 per minute, 10 per minute, 15 per minute and 30 per minute. At each of these conditions recordings were done for silent breathing (1 min) and breathing with vocalization (counting out loud) for a further minute.

Given typical conditions of controlled breathing of a healthy male, the grey and black lines in Fig. 3A shows the RR tachogram and RR deltagram based on succession of 425 RR intervals (331 s interval). The segments 1–4 of these recording indicate periods of controlled breathing at the rates of 5 (segments 1 and 2) and 10 (segments 3 and 4) breaths per minute (bpm). The length of each segment is approximately 1 min. The segments 1 and 3 correspond to silent breathing, and segments 2 and 4 to the breathing with vocalization.

To transfer these data to the frequency domain, we need to estimate fragmentary spectrum (19). Using developed algorithms, this is a standard task that is performed by the estimation of the weighting coefficients from (14) and calculation of the fragmentary spectra using (17)–(19). The corresponding fragmentary spectra are shown in Fig. 3B. The logarithmic scale of frequencies provides the means to display the spectrum for a wide range of frequencies from 0.001 to 1 Hz.

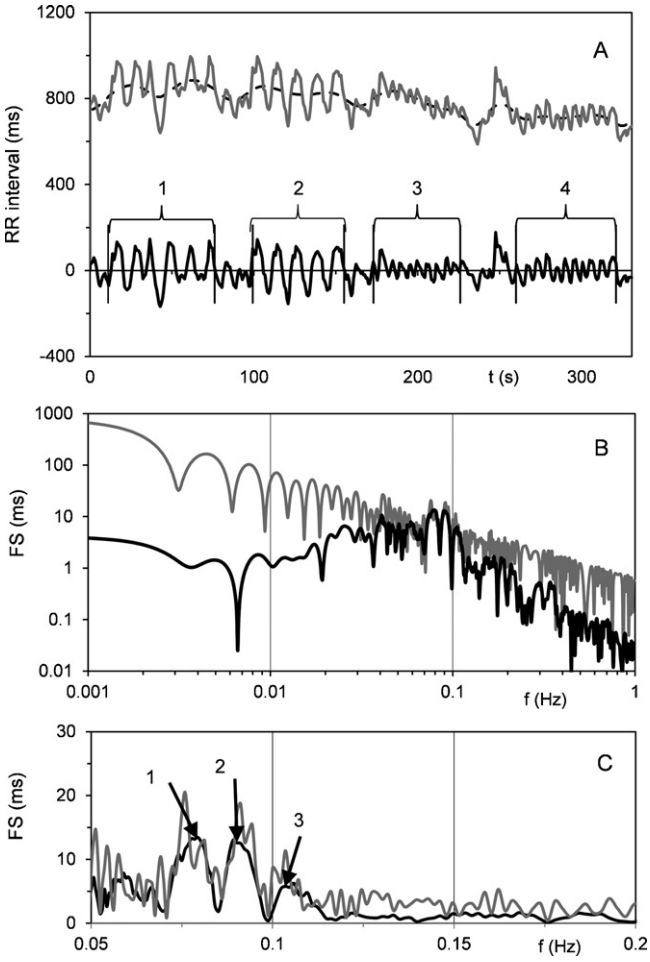

Fig. 3 – (A) Shows the deltagram (black solid line) and tachogram (grey line) based on 331 s record of 425 successive RR intervals. Dotted line: trajectory of expected values of RR intervals computed by 5 step procedure of moving averaging (21) with $n_L = n_R = 6$. The segments from 1 to 4 indicate periods of controlled breathing. (B) The black and grey lines show the fragmentary spectra of the deltagram and tachogram from (A). Here, and throughout the following illustrations, the RR measures for both tachograms and deltagrams are taken in milliseconds. Accordingly, the units of fragmentary spectrum (FS) are also milliseconds. (C) An extract from (B) which shows the spectra for a narrow frequency range from 0.05 to 0.2 Hz using natural ordinate scale.

To explain the forms of spectra, we note that in general terms the spectral analysis is associated with continuous time function $f(t)$ that extends over an infinite time scale. Conceptually, we may regard the RR tachogram as the set of the samples of such process on a finite length interval. This finite length extract from $f(t)$ may be described as $w(t) = \rho(t) \cdot f(t)$, where $\rho(t)$ is a rectangular pulse with a unit amplitude over the finite length analysis interval $[0,\lambda]$.

Fig. 4 exemplifies $w(t)$ (grey line), and shows how the RR tachogram looks over an extended time scale. In the context of continuous Fourier integrals, we deal with function that deviates from zero only over the analysis interval. These

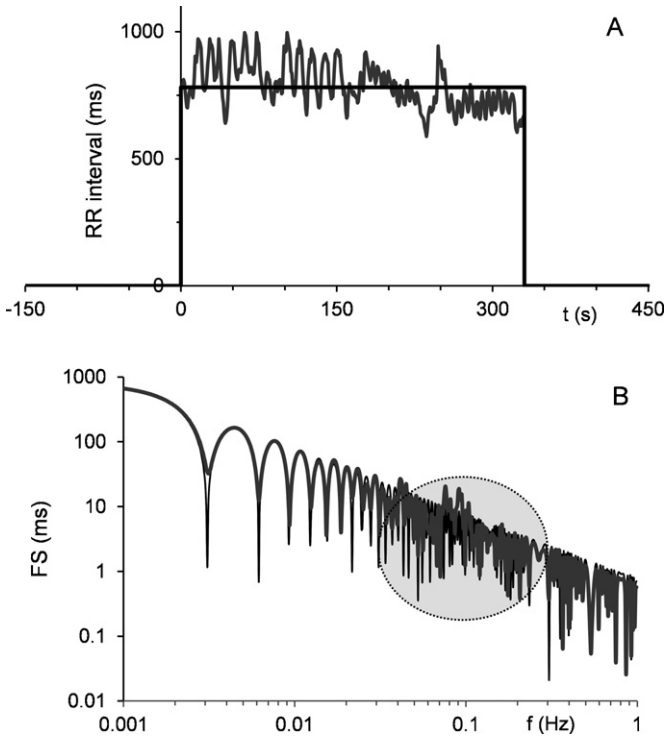

Fig. 4 – (A) Gives a visual impression of the tachogram as a finite extent function comparable with rectangle. In terms of the formula (23), the parameters of the rectangle are: A = 781 ms (mean RR interval) and λ = 331 s (length of the tachogram). (B) Compares fragmentary spectra of the tachogram and rectangle. The shadowed ellipse shows the region which reflects oscillatory components of the tachogram.

transitions create discontinuities of the process at the ends of the analysis interval.

If the length of RR intervals in question is constant, the tachogram degenerates into the rectangular impulse (solid black line) the fragmentary spectrum of which is expressed analytically in the form

$$I(f) = A\ \mathrm{sinc}(\lambda\pi f), \tag{23}$$

where A and λ are the amplitude and duration of the impulse, respectively.

For typical RR tachogram, the relative deviations of RR intervals from the mean value usually do not exceed 20–30%. For example, the mean value of RR interval of the tachogram in Fig. 4A is 781 ms, and the absolute values of the deviations do not exceed 25% of the mean. Under these conditions the RR tachogram is close to the rectangle shown in Fig. 4A by the black line. Fig. 4B shows similarity of corresponding fragmentary spectra. Consequently, the results of the tachogram spectral analysis may be completely dominated by irrelevant component (23) rather than HRV during the analysis interval.

In the general context of spectral analysis, irrelevant components are usually associated with spectral leakage [13]. The spectral distortions are due to a Fourier series model of data, the theoretical basis of the DFT and FFT. The point is that the analytical signals are defined over an infinite interval, while digitized signals are always finite in time. This distinction produces physically inconsistent components the most prominent of which is spectral leakage. Conventional reduction of spectral distortions using the windows for harmonic analysis is only effective for long-term signals. Consequently, the removal of irrelevant components in the context of the time–frequency analysis necessitates the change of the theoretical background from Fourier series to more adequate technique of integral transforms.

Previous studies employed a continuous wavelet transform as a toolkit to handle dynamical changes of HRV [16]. However, this approach comes with the significant cost of a loss of conventional frequency domain measures. Our method remains in the field of Fourier methods, and consists in the change of the theoretical background from Fourier series to Fourier integrals using a Filon-type quadrature as a computational basis [14,25]. The ability of the method to handle signal segments of arbitrary length is seen from the fact that analytical model (11) is composed from finite elements, and is in exact proximity with the finite length interval over which the PEF is defined. The SBF algorithm permits an explicit treatment of discontinuities at the boundary points. In this context, the fragmentary spectrum is equally applicable with testable accuracy to both the tachogram and deltagram.

Using the RR deltagram instead of RR tachogram, we eliminate the component (23) from the spectral analysis. Given the spectra of the deltagram and tachogram for wide range of frequencies in Fig. 3B, we note striking differences between the spectra in the ranges of low and high frequencies. Comparable parts of the spectra belong to a relatively narrow frequency range from 0.05 to 0.2 Hz. Fig. 3C shows these parts of the spectra in a more detail for the frequency diapason from 0.05 to 0.2 Hz using a natural scale of frequencies. The point which emerges is that the fragmentary spectrum of the tachogram contains multiple peaks some of which are likely to be relevant to the component (23). The form of the fragmentary spectrum of the deltagram is more informative, and contains 3 major resonant peaks indicated by the arrows 1, 2 and 3. The corresponding resonant frequencies are: 1, 0.079 Hz; 2, 0.089 Hz; 3, 0.106 Hz. However, the justification of these peaks as functionally meaningful components is complicated by the lack of global stationarity of the data under the analysis. A nonhomogenous character of the deltagram is easily recognised by the visual analysis. It is clearly seen from Fig. 3A that slow high amplitude oscillatory components (segments 1 and 2) are followed by faster oscillatory components with significantly lower amplitudes (segments 3 and 4). Given that HRV develops over these segments simultaneously with controlled respiration, we may associate oscillatory components of HRV with the breathing rhythms of 5 bpm (0.083 Hz) and 10 bpm (0.167 Hz), respectively. However, there is no evidence of a 10 bpm rhythm in the profile of the fragmentary spectrum. Either of the peaks 1 and 2 may be related to the respiratory rhythms of 5 bpm. To make unambiguous conclusions, we obviously need a more precise analysis which can tell us about the timing of the sources of oscillatory components. For this purpose we now apply spectral analysis to the segments 1 and 3 (controlled silent breathing) in Fig. 3A. The corresponding RR deltagrams are presented in Fig. 5A and B by the data points displayed as

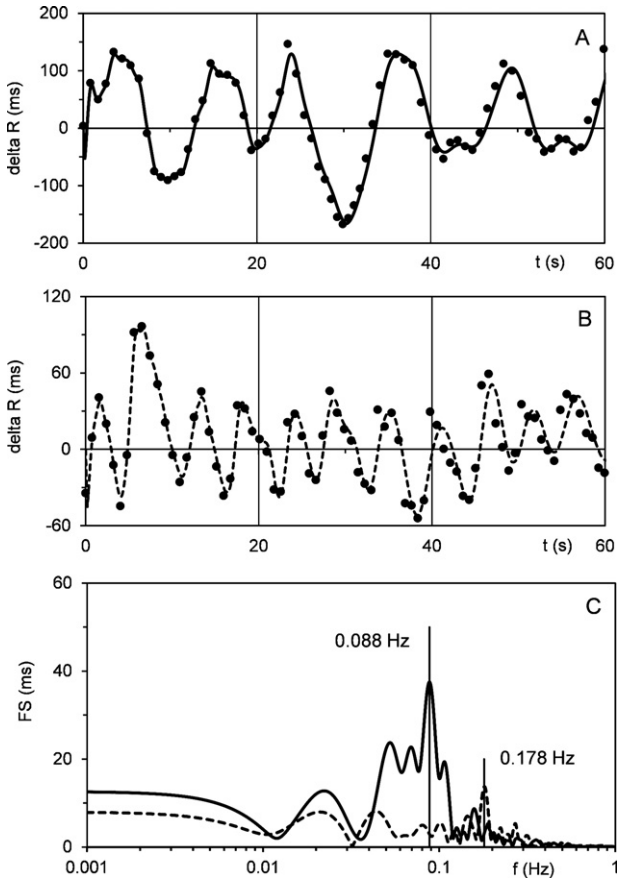

Fig. 5 – (A) The segment 1 of the deltagram from Fig. 3A is displayed by the filled circles. The time to frequency and frequency to time Fourier transformations of these data points restore initial discrete deltagram in the form of continuous time function (solid line). (B) The filled circles display the segment 3 of the deltagram from Fig. 3A. The dotted line shows continuous deltagram estimated by the time to frequency and vice versa Fourier transforms. (C) The solid and dotted lines show the fragmentary spectra computed from the data points displayed in (A) and (B), respectively. The vertical lines show dominant resonant peaks located in the frequency ranges of controlled breathing.

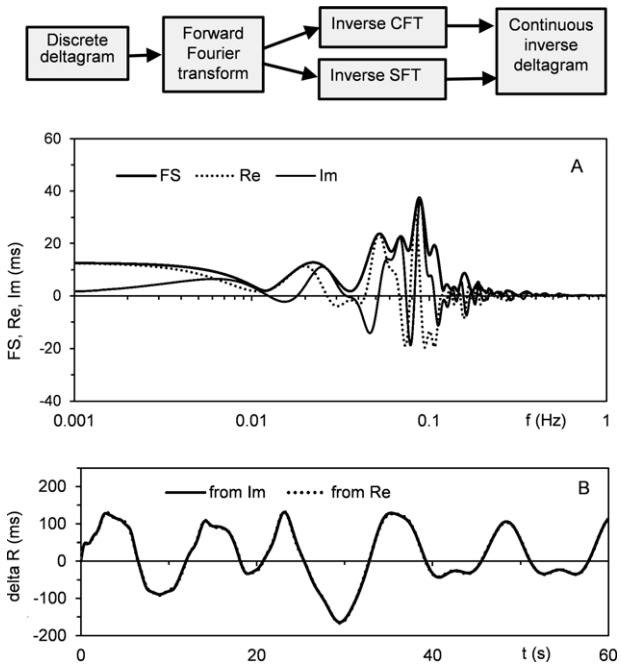

Fig. 6 – Upper block diagram shows that forward Fourier transform produces the two frequency domain counterparts of discrete RR deltagram. From these functions inverse cosine Fourier transform (CFT) and inverse sine Fourier transform (SFT) restore original deltagram in the form of continuous time function. (A) The solid line is the fragmentary spectrum reproduced from Fig. 5C. The dotted and grey lines show the real and imaginary parts of the corresponding complex spectrum. (B) Shows continuous deltagrams computed from the real and imaginary parts of the complex spectrum.

the filled circles. It is important to note that we have defined the RR deltagram as a discrete finite extent function. In this context the discrete sequence of the data points is an exact graphical form of RR deltagram.

The fragmentary spectra of the deltagrams are shown in Fig. 5C. It is widely accepted to regard a peak in the Fourier spectrum as the indication of an oscillatory component in the temporal structure of the underlying signal. Multiple peaks do not necessarily mean that several oscillations are present. They can be related to different factors that diverge a real oscillatory component from an ideal sine wave.

A characteristic feature of both spectra is the presence of well-pronounced resonant peaks: at 0.088 Hz for the segment 1 and at 0.178 Hz for the segment 3. In both spectra these peaks dominate over multiple peaks with significantly smaller amplitudes. Fragmentary spectra from segments 2 and 4 (controlled breathing with vocalization) have similar resonant peaks at the frequencies 0.08 and 0.177 Hz, respectively. The agreement between the frequencies of these dominant peaks of fragmentary spectra, and the frequencies 0.083 and 0.167 Hz of the corresponding breathing rhythms leads us to conclude that we are indeed observing a coordination of cardiac and respiratory systems.

The reconstruction of inverse RR deltagram using inverse Fourier transforms is the further step toward the establishment of the links between the time and frequency domains of the signal. The solid line in Fig. 5A and dotted line in B are the inverse deltagrams computed from the real parts of the corresponding complex spectra. By contrast to the digital RR deltagram, the inverse RR deltagram can be computed at arbitrary chosen time points, and thus may be treated as a continuous time function. From this figure, we see an excellent agreement of continuous deltagram with the data points of original discrete RR deltagram.

The block diagram in Fig. 6 illustrates the major steps through which a discrete RR deltagram is transformed into the form of a continuous time function. An essential point is that the time to frequency transformation produces the two frequency domain counterparts of the original deltagram. Both

the real and imaginary parts of the complex spectrum contain full amount of amplitude and phase information which is necessary to restore the original time function. Given the RR deltagram from Fig. 5A, Fig. 6A exemplifies the real and imaginary parts of the corresponding complex spectrum. These functions behave in a more complex manner than the fragmentary spectrum (solid line) reproduced from Fig. 5C.

For the purpose of inverse transformations, the real and imaginary part functions were presented by the sequences of evenly spaced samples in the logarithmic scale of frequencies extending from 0.001 to 1 Hz. The sampling rate was established at the level that provided 200 samples per decade, i.e. overall 601 sample for each function. Standard calculations of numerical Fourier transforms have been facilitated by effective procedures of the fast SBF algorithm [14].

Fig. 6B shows inverse RR deltagrams computed from the real and imaginary part functions. In the scales of this figure the plots of numerical solutions are indistinguishable one from another.

The definition of inverse RR deltagram specifies accuracy of inverse transforms by the components $r_{IC}(t)$ and $r_{IS}(t)$ in the error functions (22). A practical coincidence of numerical solutions produced by the real and imaginary part functions suggests that the errors of inverse transforms are negligibly small compared with the errors of the estimates of the fragmentary spectra. Therefore, a low level of summary errors provides evidence of reliability and very satisfactory accuracy with which the developed algorithms estimate fragmentary spectra.

5.2. *Identification of a transient oscillatory component*

Here we consider ability of the time–frequency analysis to detect and identify specific TOC of HRV using the dominant frequency as descriptive frequency domain measure of the fragmentary spectrum. Given conditions of controlled breathing, Fig. 7 shows the deltagram of heartbeats on the 200 s interval during which the breathing rate of 15 bpm (segment 1) was followed by the breathing rate of 30 bpm (segment 3). The length of each breathing interval was about 1 min. The fragmentary spectra computed from these segments are shown in Fig. 7B and C by the solid lines. The fragmentary spectra were also computed from shorter segments 2 and 4, and displayed in Fig. 7B and C by the grey lines. The vertical dashed lines indicate spectral peaks the frequencies of which can be associated with the frequencies of breathing. Thus, the changing profiles of fragmentary spectra reveal the frequency and timing of oscillatory components which can be unambiguously associated with the rhythms of controlled breathing. This finding of TOCs is consistent with the evidence of strong coupling between the rhythms of respiration and HRV supported by different quantitative methods [29,30]. Physiological aspects of this paradigm are known as the respiratory sinus arrhythmia [8].

Comparison of the fragmentary spectra from Fig. 5C, Fig. 7B and C shows that amplitudes of resonant peaks associated with controlled breathing decrease with increase of the frequency. This development is accompanied by progressive complication of spectral characteristics. Fig. 5C shows that resonant peak induced by the breathing rhythm of approximately 5 bpm (0.088 Hz resonant peak) is a dominant component of the fragmentary spectrum. By contrast, the resonant peaks associated with 15 and 30 bpm breathing rhythms (Fig. 7B and C) are mixed with a number of transient components the origins of which is difficult to trace. The change of the parameters of the fragmentary spectrum has significant effect on the spectral estimates, particularly the amplitude of the spectral peak underlying the TOC. In this situation the resonant frequency appears as a relatively stable parameter. This supports a dominant resonant frequency as a descriptive parameter of TOC.

The deltagram used to exemplify the temporal evolution of this parameter, is illustrated by Fig. 8A. This is a piece of the deltagram from Fig. 3A which includes the segments 2 and 3. The moving window analysis has been supported by the following parameters:

- Initial and final positions of the pointer: sample 1 ($t = 0$) and sample 210 ($t = 165$ s).
- Increment for the change of pointer position: 1.
- The range of the tested frequencies: from 0.04 to 0.5 Hz.
- Sampling rate in the logarithmic scale: 200 samples per decade.

These parameters were implemented in different trials using windows with different numbers of data points. Because the time points of the RR deltagram are non-uniformly spaced, the length of the window may take different values depending on the position of the pointer. During each trial the pointer takes the positions of subsequent time points of the deltagram, and at each point the frequency domain routines calculate the fragmentary spectrum for the frequencies of interest from 0.04 to 0.5 Hz (230 points), and estimate its maximum value. The frequency of this largest resonant peak supports each data point of the tachogram through the value of the dominant resonant frequency.

Fig. 8B shows the plots of dominant frequencies which were obtained using 50 (solid line) and 40 (dotted line) point windows. These are typical results which indicate that moving window fragmentary spectral analysis provides stable results, and reliably identifies time–frequency parameters of TOCs.

The choice of the window parameters should be linked to the expected frequency of TOCs. Given M point window, the value of its mean length may be evaluated as $T_W = M \cdot \overline{RR}$, where $\overline{RR}$ is the mean of the RR intervals in the underlying deltagram. For the deltagram from Fig. 8A $\overline{RR} \approx 0.8$ s. Consequently, the mean lengths of 40 and 50 point windows are approximately 32 and 40 s. Computer experiments with different window parameters suggest that $T_W > 3\,T_D$ may be regarded as condition that provides reliable identification of TOC with dominant frequency $f_D = 1/T_D$, where T_D is the period of the oscillation. In this context, Fig. 8B indicates that both 40 and 50 point windows provide similar results.

The distributions of dominant frequencies are summarised by the histogram in Fig. 8C. The manner in which the distributions develop clearly indicates the two groups of frequencies which are separated by the dashed vertical line. The mean frequencies for the low frequency range are: 0.08 Hz (123 samples, 50 point window), and 0.082 Hz (124 samples, 40 point window). The similar data for the high frequency range:

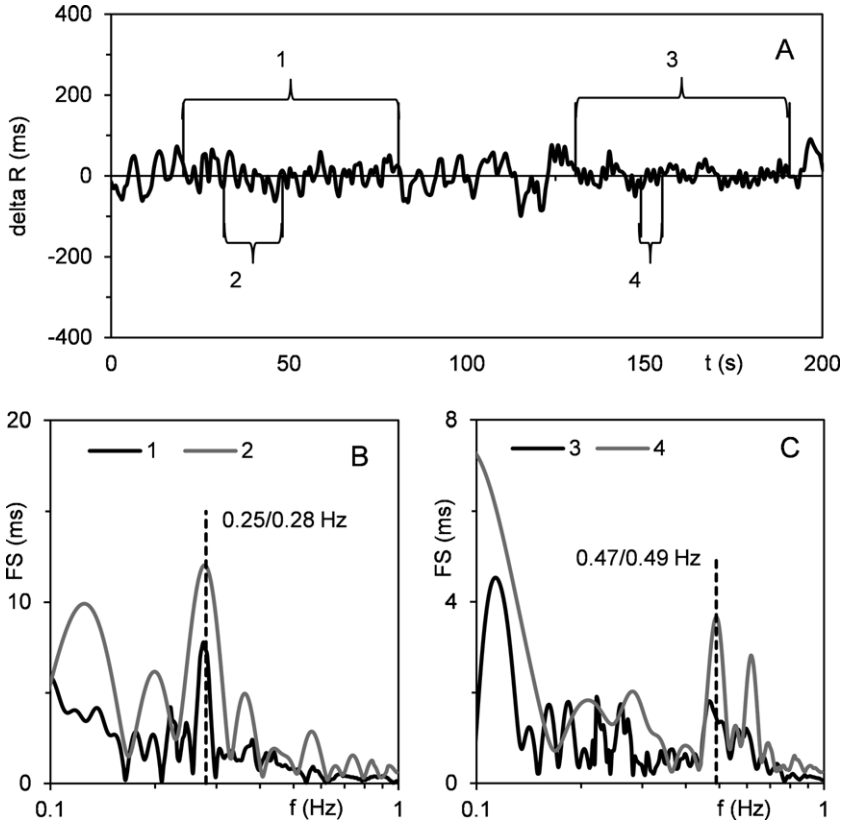

Fig. 7 – (A) Deltagram based on 200 s record of 250 successive RR intervals. Segments 1 and 3 indicate two successive periods of controlled breathing with 15 bpm and 30 bpm rates. Segments 2 and 4 specify shorter segments within each of these periods. (B) Black and grey lines show fragmentary spectra computed from segments 1 and 2. (C) Black and grey lines show fragmentary spectra computed from segments 3 and 4.

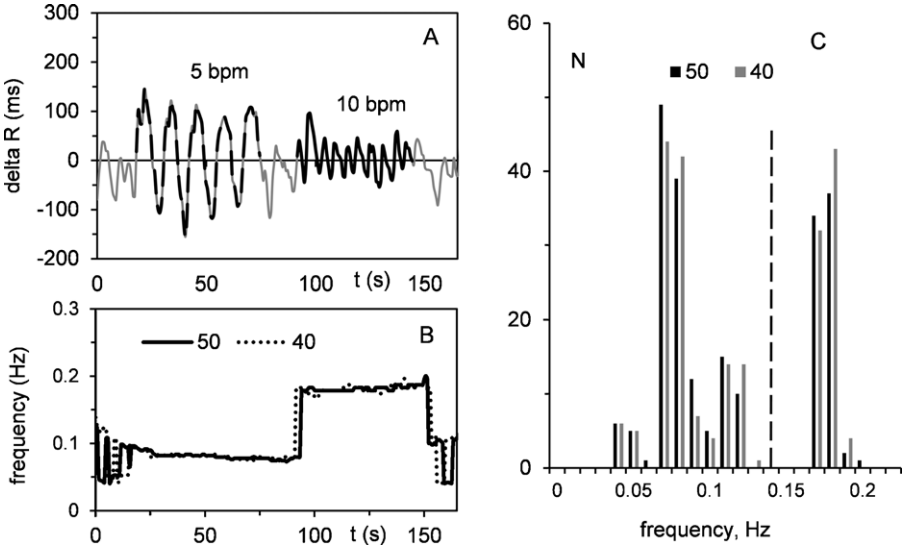

Fig. 8 – Illustrates the identification of transient oscillatory components of HRV induced by controlled breathing. (A) 210 data point RR deltagram. The segments highlighted by the bold dotted and solid lines show periods of controlled breathing with the rates of 5 and 10 bpm. (B) Shows dominant frequencies of the fragmentary spectra estimated by a moving window procedure with 50 (solid line) and 40 (dotted line) point windows. (C) Histogram with 0.01 Hz bin shows distributions of the estimated dominant frequencies. The height of column is the number of dominant frequencies identified within the corresponding bin.

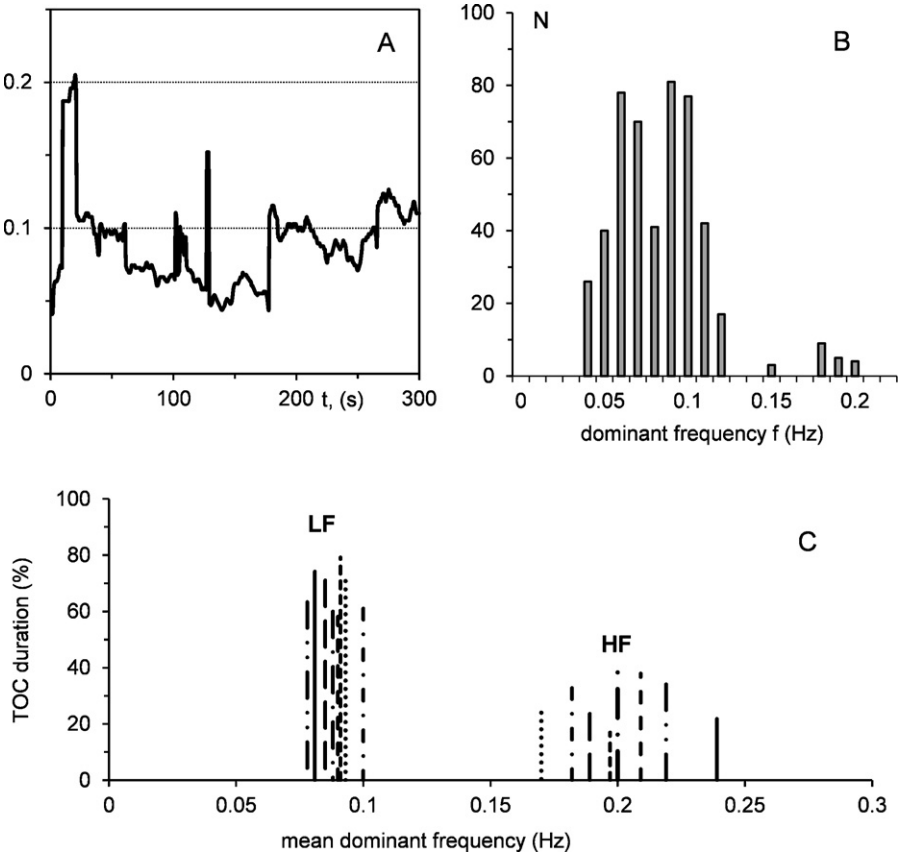

Fig. 9 – (A) Shows the trajectory of dominant frequencies estimated by the fragmentary spectral analysis from 300 s RR deltagram using 50 point moving window. (B) Illustrates the distribution of dominant frequencies in the same manner as the histogram in the previous figure. (C) Illustrates durations of TOCs with dominant LF and HF components identified from real-life HRV data of 8 healthy subjects. For each subject the same type of the line is used for LF and HF ranges.

0.182 Hz (87 samples, 50 point window), 0.181 Hz (86 samples, 40 point window). We have two good reasons for considering the dominant frequency as a robust marker of TOC. One is the fact that estimates of dominant frequencies are remarkably stable under unavoidable amplitude variations of the TOCs. Our other reason for appreciation of this marker is stability of the estimates obtained from the windows of different length.

Fig. 9 shows similar results for HRV recorded under the real-life, i.e. uncontrolled conditions. In this case the moving window analysis identifies multiple TOCs of different frequencies, duration and timing. These TOCs may be regarded as quasi-stationary elements of non-stationary HRV. An important finding is that dominant frequencies of these elements may be associated in some cases with conventional LF and HF frequency bands of HRV. A typical situation of this kind is illustrated by Fig. 9. The trajectory of dominant frequencies in Fig. 9A shows the results of the moving window fragmentary spectral analysis of 300 s RR deltagram (468 data points).

The histogram in Fig. 9B shows that distribution of dominant frequencies can be divided into the two distinct parts separated by the vertical dashed line. The mean dominant frequency for the low frequency range is 0.083 Hz (447 samples). For the high frequency range the mean dominant frequency is 0.187 Hz (21 samples). These mean frequencies belong to functionally meaningful LF and HF bands identified in the studies of HRV power spectra [3,7,9].

The elements of LF and HF bands have been considered in the previous studies as continuous processes produced by stationary systems. An important advantage of our approach is that division of the deltagram into TOCs provides means to disclose the temporal dynamics of LF and HF elements. We illustrate this capability of the method using the real-life HRV data from 8 healthy subjects participated in the study. For each subject the moving window analysis (20 point window) was applied to 5 min segment of the deltagram. Given TOC at particular position of the window, the dominant frequency in the range from 0.04 to 0.13 Hz was qualified as LF element, and in the range from 0.135 to 0.5 Hz as HF element. Using identified ensembles of LF and HF elements, for each subject the mean dominant frequencies have been estimated. These frequencies are indicated in Fig. 9C by vertical lines, separately for LF and HF ranges. The height of the line shows the percent of the time, relative to the length of the deltagram, during which the corresponding elements were identified. This evidence of complex time-varying properties of HF and LF elements indicates that cardiovascular regulatory mechanisms are activated at different time instants, and can be associated with different control scenarios. The consistent relationship is the longer durations of LF elements (mean = 64.5, variance = 7.3)

compared with durations of HF elements (mean = 30.2, variance = 7.9).

6. Discussion

This work has focused on the development of new methods for extracting information from HRV data using simultaneous consideration of HRV measures in both the time and frequency domains. The necessity for significant improvements of the methods of HRV spectral analysis relates to the fact that the power spectrum, the recommended and most commonly used frequency domain characteristic of HRV [3], is a concept and tool addressed to stationary processes, whereas in fact, the consideration of HRV as a stationary process is a gross oversimplification.

Over recent years time–frequency analysis has emerged as the most favoured approach to improve the analysis and interpretation of the changing spectral composition of non-stationary HRV [9,11,12]. Being underpinned by ideas of the time–frequency analysis, the design of main algorithms reported in this paper depended critically on the methodological innovation of short time spectral analysis provided by the SBF algorithm [14]. The problem is that short term spectral analysis is highly sensitive to spectral leakage that can cause totally unacceptable distortions of the spectral estimates. Therefore, the added spectral information gained needs to be balanced by a full appreciation of the accuracy of spectral estimates. Conventional evaluation of numerical algorithms consists in comparison of computational results with theoretical models. Unfortunately, there is insufficient detailed physiological knowledge to describe HRV in terms of adequate mathematical models pertinent for both the time and frequency domains. Artificial time-domain sequences of RR intervals used in the previous studies to test the algorithms are not supported by the corresponding frequency domain solutions [9,10,17,18]. There is simply no frequency domain "gold standard" to which the HRV spectral estimates can be compared to establish the veracity of different algorithms.

Since the frequency domain judgements are not available, we have relocated the analysis of accuracy from the frequency to the time domain. This was made using the convertibility of the time to frequency and frequency to time Fourier transforms. Once the spectrum is calculated, the inverse transform recovers the original function and reveals computational accuracy. According to this analysis, we demonstrate that the accuracy with which the original function is recovered from the fragmentary spectrum is very satisfactory and may be regarded as strongly supportive of the suitability of the developed algorithms for the time–frequency analysis of HRV. Thus, the fragmentary spectrum introduced in this study allows high resolution of the signal in the frequency plane, which is necessary for the accurate identification and partitioning of pertinent components of HRV. In this way both the frequency content, timing and duration of HRV segment of interest can be captured together by the fragmentary spectrum.

However, it is important to note that extraction of short time fragments from conventional RR tachogram creates a situation illustrated by Fig. 4. It appears that the time function to be transformed is close to the rectangular pulse. The corresponding spectrum dominates in the results of short time–frequency analysis. We overcome this problem by the introduction of the RR deltagram. The expected trajectory of RR intervals is estimated by the algorithm of a multistep moving window averaging by which we extend conventional moving window averaging to the treatment of a non-evenly sampled signal in question.

These refinements in the technique of HRV non-stationary spectral analysis provide means for better recognition and understanding of the sources of the different oscillatory components of HRV. The previous solutions based on the measurements of the power spectrum are limited by constraints imposed by the condition of stationarity, and include two compulsory assumptions. First, the component is continuously produced by a system the parameters of which remain unchanged during the whole epoch of analysis. Second, HRV develops via a process of linear summation of different components generated by functionally independent sources.

These backgrounds have shaped virtually every aspect of conventional HRV spectral analysis, from the types of explanations proposed for functional and clinical significance of power spectra, to the way in which the HRV is reconstructed in computer simulations [9,17]. However, converging evidence from empirical observations suggests that cardiovascular oscillations are complex and mutable, and various cardiovascular control scenarios may be activated at different time instants, and hold features that reflect the underlying physiological mechanisms [31].

The coupling between respiratory and cardiac systems has been described historically as respiratory sinus arrhythmia [8]. The experimental data obtained in this study in controlled breathing conditions show that the breathing rhythm is reflected in the RR deltagram by an oscillatory component of the corresponding frequency. If the breathing rate is unchanged during several breath periods, the induced oscillatory component plays a dominant role in the profile of the corresponding fragmentary spectrum. Therefore, regular breathing is able to suppress the harmonic components from LF or/and HF ranges. This finding of irregularities in the generation of oscillatory components from LF and HF ranges is further supported by the experimental data from uncontrolled, real-life conditions. Although in some instances the transient oscillations are most pronounced in LF and HF ranges, more typically the temporal overlap of corresponding activities is highly complex and irregular.

More studies will be needed to take advantage of the power of novel fragmentary spectral analysis techniques. An important goal is devising joint time–frequency distributions that play a crucial role in the understanding of time varying spectra [32]. Being based on physical considerations of underlying processes, the design of such distributions is supported by remarkable variety of heuristic approaches. Our finding of a specific oscillatory component of HRV linked to the rhythm of respiration may serve as a guideline to a specific distribution. The results presented in this paper provide the core of the approach.

REFERENCES

[1] R.I. Kitney, O. Rompelman, The Study of Heart Rate Variability, Oxford University Press, Oxford, UK, 1980.

[2] A. Malliani, Association of heart rate variability components with physiological regulatory mechanisms, in: M. Malik, A.J. Camm (Eds.), Heart Rate Variability, Futura, New York, NY, 1995, pp. 173–188.

[3] Task Force of The European Society of Cardiology, The North American Society of Pacing, Electrophysiology, Heart rate variability standards of measurement, physiological interpretation, and clinical use, European Heart Journal 17 (1996) 354–381.

[4] M.P. Tulppo, T.H. Makikallio, T.E.S. Takala, T. Seppanen, H.V. Huikuri, Quantitative beat-to-beat analysis of heart rate dynamics during exercise, American Journal of Physiology 271 (1996) H244–H252.

[5] M.A. Austin, T.C. Riniolo, S.W. Porges, Borderline personality disorder and emotion regulation: insights from the polyvagal theory, Brain and Cognition 65 (2007) 69–76.

[6] U.R. Acharya, K.P. Joseph, N. Kannathal, C.M. Lim, J.S. Suri, Heart rate variability: a review, Medical and Biological Engineering and Computing 44 (2006) 1031–1051.

[7] S. Akselrod, D. Gordon, F.A. Ubel, D.C. Shannon, A.C. Barger, R.J. Cohen, Power spectrum analysis of heart rate fluctuation: a quantitative probe of beat-to-beat cardiovascular control, Science 213 (1981) 220–222.

[8] G.G. Berntson, J.T. Bigger Jr., D.L. Eckberg, P. Grossman, P.G. Kaufmann, M. Malik, H.N. Nagaraja, S.W. Porges, J.P. Saul, P.H. Stone, M.W. van der Molen, Heart rate variability: origins, methods, and interpretive caveats, Psychophysiology 34 (1997) 623–648.

[9] Y. Goren, L.R. Davrath, I. Pinhas, E. Toledo, S. Akselrod, Individual time-dependent spectral boundaries for improved accuracy in time–frequency analysis of heart rate variability, IEEE Transactions on Biomedical Engineering 53 (2006) 35–42.

[10] V. Shusterman, B. Aysin, K.P. Anderson, A. Beigel, Multidimensional rhythm disturbances as a precursor of sustained ventricular tachyarrhythmias, Circulation Research 88 (2001) 705–712.

[11] A. Monti, C. Médigue, L. Mangin, Instantaneous parameter estimation in cardiovascular time series by harmonic and time–frequency analysis, IEEE Transactions on Biomedical Engineering 49 (2002) 1547–1556.

[12] B. Aysin, L.F. Chaparro, I. Gravé, V. Shusterman, Orthonormal-basis partitioning and time–frequency representation of cardiac rhythm dynamics, IEEE Transactions on Biomedical Engineering 52 (2005) 878–889.

[13] E.O. Brigham, The Fast Fourier Transform, Prentice-Hall, New York, NY, 2002.

[14] D. Melkonian, Similar basis function algorithm for numerical estimation of Fourier integrals, Numerical Algorithms 54 (2010) 73–100.

[15] R.W. DeBoer, J.M. Karemaker, J. Strackee, Comparing spectra of a series of point events particularly for heart rate variability data, IEEE Transactions on Biomedical Engineering 31 (1984) 384–387.

[16] R.D. Berger, S. Akeselrod, D. Gordon, R.J. Cohen, An efficient algorithm for spectral analysis of heart rate variability, IEEE Transactions on Biomedical Engineering 33 (1986) 900–904.

[17] G.D. Clifford, L. Tarassenko, Quantifying errors in spectral estimates of HRV due to beat replacement and resampling, IEEE Transactions on Biomedical Engineering 52 (2005) 630–638.

[18] J. Mateo, P. Laguna, Improved heart rate variability signal analysis from the beat occurrence times according to the IPFM model, IEEE Transactions on Biomedical Engineering 47 (2000) 985–996.

[19] R.H. Clayton, S.W. Lord, J.M. McComb, A. Murray, Comparison of autoregressive and Fourier transform based techniques for estimating RR interval spectra, Computational Cardiology (1997) 379–382.

[20] G.B. Moody, Spectral analysis of heart rate without resampling, Computational Cardiology (1993) 715–718.

[21] A. Broadman, F.S. Schlindwein, A.P. Rocha, A. Leite, A study on the optimum order of autoregressive models for heart rate variability, Physiological Measurement 23 (2002) 324–336.

[22] D. Melkonian, E. Gordon, C. Rennie, H. Bahramali, Dynamic spectral analysis of event-related potentials, Electroencephalography and Clinical Neurophysiology 108 (1998) 251–259.

[23] D. Melkonian, T. Blumenthal, E. Gordon, Numerical Fourier transform spectroscopy of EMG half-waves: fragmentary-decomposition-based approach to nonstationary signal analysis, Biological Cybernetics 81 (1999) 457–467.

[24] D. Melkonian, T. Blumenthal, R. Meares, High resolution fragmentary decomposition—a model based method of non-stationary electrophysiological signal analysis, Journal of Neuroscience Methods 131 (2003) 149–159.

[25] A. Iserles, On the numerical quadrature of highly-oscillatory integrals. I. Fourier transforms, IMA Journal of Numerical Analysis 24 (2004) 1110–1123.

[26] B. Noble, Variational finite element methods for initial value problems, in: J.R. Whiteman (Ed.), The Mathematics of Finite Elements and Applications, Academic Press, London/New York, 1973, pp. 143–151.

[27] A. Papoulis, Probability, Random Variables, and Stochastic Processes, McGraw-Hill, New York, 2002.

[28] W.H. Press, B.P. Plannery, S.A. Teukolsky, W.T. Vetterling, Numerical Recipes in C: The Art of Scientific Computing, Cambridge University Press, Cambridge, UK, 1993.

[29] F. Censi, G. Calcagnini, S. Cerutti, Coupling patterns between spontaneous rhythms and respiration in cardiovascular variability signals, Computer Methods and Programs in Biomedicine 68 (2002) 37–47.

[30] O. Meste, B. Khaddoumi, G. Blain, S. Bermon, Time-varying analysis methods and models for the respiratory and cardiac system coupling in graded exercise, IEEE Transactions on Biomedical Engineering 52 (2005) 1921–1930.

[31] M. Cohen, J.A. Taylor, Short-term cardiovascular oscillations in man: measuring and modelling the physiologies, Journal of Physiology 542 (3) (2002) 669–683.

[32] L. Cohen, Time–frequency distributions—a review, in: Proceedings of the IEEE 77, 1989, pp. 941–981.